Lab 6 Report: Path Planning and Following Utilizing A*, Monte Carlo Localization, and Pure Pursuit

Team 3

Thomas Buckley
Fiona Wang
Sriram Sethuraman
Ben Lammers

6.4200 RSS

April 18, 2025

1 Introduction

Ben Lammers

As we continue to develop our racecar to perform more complex tasks, the ability to navigate between locations will become increasingly valuable. In Lab 6, our objective was to implement a full navigation stack that combines localization, path planning, and control to move a racecar from a known starting location to a specified goal.

We built upon our previously developed Monte Carlo localization (MCL) algorithm, which estimates the racecar's pose using a set of particles. Each particle represents a potential location and orientation of the racecar, and we update their positions based on motion data and evaluate them against real-time LiDAR scans to match features in a known map.

With localization in place, we focused on path planning. Given a known map and a target goal, we aimed to compute a sequence of waypoints that guides the racecar along a collision-free path. We experimented with both sampling-based (RRT) and search-based (A*) algorithms to generate these paths. Once a path was generated, we pass it to a pure pursuit controller, which calculates steering commands that enable the racecar to follow the path smoothly.

Our success criterion for this lab was straightforward: the racecar should follow an efficient and collision-free path from the start to the goal using the combined outputs of localization, planning, and control.

As our platform for development, test, and evaluation, we continue to use the same racecar for this lab as in past labs, which is a 4-wheel (front-wheel steering racecar) powered by an NVIDIA Jetson running ROS2.

2 Technical Approach

Ben Lammers, Sriram Sethuraman, Fiona Wang

The technical task consisted of both a localization problem and a path planning problem. For localization, we needed to publish the real-time position of the racecar on a provided map, given an initial position guess, odometry data, and LiDAR data. Our approach relied on the Monte Carlo localization method, which started with 200 particles, iteratively updating them using a motion model and sensor model. For path planning, we developed and tested both an A* search-based algorithm and an RRT sample-based algorithm, and paired those algorithms with a pure pursuit controller to follow the path.

2.1 Monte Carlo Localization

2.1.1 Motion Model

The motion model uses odometry data to update our current particles so that they reflect the movement of the racecar. The model takes in an array of particles, as well as odometry data, including estimated changes in position (Δx, Δy, $\Delta\theta$) in the body frame of the racecar. This array is either from the previous iteration's particle filter (described below) or sampled from a normal distribution centered at our initial guess position.

After receiving the array of particles, the motion model uses odometry data to generate updated particle positions. To account for uncertainty in the odometry readings, we add noise to the transformation equations. The final equations are:

$$x_{i+1} = x_i + (\Delta x + \varepsilon_x)\cos\theta_i - (\Delta y + \varepsilon_y)\sin\theta_i \tag{1}$$

$$y_{i+1} = y_i + (\Delta x + \varepsilon_x)\sin\theta_i + (\Delta y + \varepsilon_y)\cos\theta_i \tag{2}$$

$$\theta_{i+1} = \theta_i + \Delta\theta + \varepsilon_\theta \tag{3}$$

As we can see above, the racecar's motion data are transformed by the previous estimate of θ, denoted by θ_i. We also add noise (ε) sampled from a normal distribution for x, y, and θ:

$$\varepsilon \sim \mathcal{N}(0, \sigma^2) \tag{4}$$

The standard deviation used for our normal distribution, σ, was found experimentally by testing multiple values in simulation, which is discussed further Section 3.1. The output of the motion model is a new set of particles, each representing a hypothesis for the racecar's current position and orientation, which are then passed to the sensor model.

2.1.2 Sensor Model

The goal of the sensor model is to determine the probability that each particle is the pose of the racecar. To do this, we are given the map, the racecar's most recent LiDAR scan, and the current particles poses as inputs. The output is an array containing a probability corresponding to each particle. This component is essential for our particle filter to be able to accurately localize itself without relying on pure dead reckoning, which is prone to accumulated error.

To do that we generate what each particle would see in LiDAR, and compare that with the real LiDAR data. At each particle, we multiply all the individual probabilities of each LiDAR beam matching the measured value (obtained using look-up table). We then normalize and return this array of probabilities to the particle filter.

2.1.3 Particle Filter

Our final task for our Monte Carlo localization method was to assemble our particle filter using our motion and sensor model. First, we select an initial pose using the 2D Post Estimate tool in RViz. Using the selected pose, we initialize our particles using a multivariate normal distribution surrounding the chosen point.

After initializing, our odom_callback function determines the change in position using the twist component of the OdometryMessage. Inputting the change in position, we update the particles using the motion model explained above. Next, our laser_callback function takes a laser scan and first, downsamples the number of scans from 1000 to 99 to reduce ray casting. The callback function then computes the probabilities using our sensor model, raises the output by a power of $\frac{1}{3}$, and normalizes the probabilities. By raising the probabilities to a power of $\frac{1}{3}$, we were able to "squash" and spread out the probabilities, preventing premature convergence.

Finally, we publish our new pose in our publish_pose function by finding the 'average' position. To do this, we find the weighted average of the x and y values based on our probabilities and find the circular mean for our θ value, which is shown below:

$$\theta = \text{atan2}(\frac{1}{n}\sum_{j=1}^{n}\sin(\alpha_j), \frac{1}{n}\sum_{j=1}^{n}\cos(\alpha_j)) \tag{5}$$

2.2 Path Planning

For the path planning portion of our navigation stack, we decided to implement and analyze both a sample based planning algorithm called RRT and a search based planning algorithm called A*. To evaluate these algorithms, we implemented them, evaluated their performances, ultimately choosing to apply A* to our racecar.

2.2.1 A* Planning Algorithm

Our implementation of A* is a search-based planning algorithm that works by converting our map into a discrete graph and searching for the shortest discrete path through that graph to the goal.

To start, our algorithm adds a buffer to our map, to provide a minimum distance from the wall for planning purposes. Using SciPy's dilation function, we add 10 iterations of dilation to our provided occupancy grid, resulting in 10 pixels of a buffer around obstacles. Next, our algorithm discretizes and downscales the occupancy grid by downscaling, turning each 10x10 pixel block into a single-pixel block (where each single-pixel is the maximum occupancy value in the 10x10 grid). Next, we connect each adjacent non-occupied grid pixel as a node in a graph, as we see in Fig. 1 below.

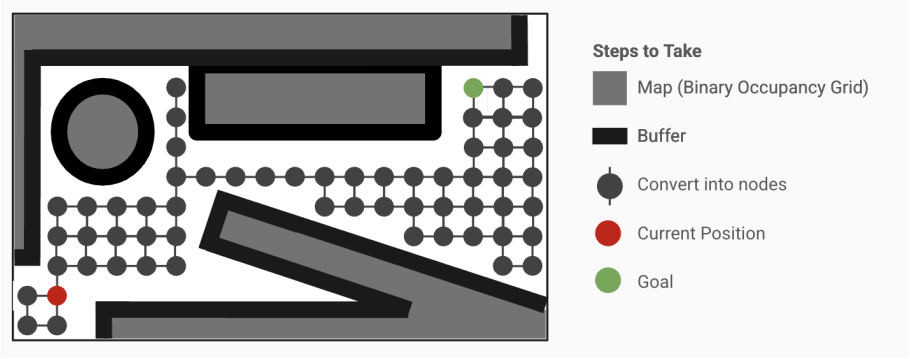

Figure 1: The map (in gray) is downscaled into a graph with connected nodes, which enables A* to search the graph.

After the graph is created, we run an A* search starting from the current position and search for the goal. The A* algorithm explores nodes in the order that they minimize the objective function $f(n)$:

$$f(n) = g(n) + h(n) \tag{6}$$

In this equation, $g(n)$ represents the accumulated cost (number of nodes along the path to get to this node), and $h(n)$ is a heuristic, which in this case is the

Euclidean distance to the goal:

$$h(n) = \sqrt{(x_n - x_{goal})^2 + (y_n - y_{goal})^2} \tag{7}$$

$h(n)$ is always less than the true cost to the goal, since the true cost is at least the Manhattan distance, which is always greater than the Euclidean distance. Thus $h(n)$ is an admissible heuristic, so once (using this objection function), A* has finally reached the goal through exploration, the search-algorithm simply traces back the path to the goal, based on which node each prior node was explored from.
The primary advantage of A* is that it is guaranteed to return the most optimal path to a goal state (if one exists). The primary disadvantage of A* is runtime $O(b^d)$, where b is the branching factor 3, and d is the length of the solution (in number of edges). Given the high number of edges in the graph, this grows quite fast, with quantitative results discussed in Section 3.2

2.2.2 RRT Planning Algorithm

The overall strategy of RRT is to grow a tree by randomly sampling our space and connecting the feasible paths to our tree until we reach our goal location. To tackle this task, we start from our given start position and randomly generate new nodes using a uniform distribution. To help our tree grow towards the goal position, we implemented a goal bias that returns the goal position instead of a random node 10% of the time, helping push our tree in the correct direction. After generating a random node, we find the nearest pre-existing node in our tree and create a node along the edge between the random and current node that is a set "step" distance from the current node. This "step" distance is a parameter that we tuned while testing our algorithm, and it controls the resolution of our path; a smaller step size creates a bumpier path while larger step size utilizes longer, straighter lines. This process can be visualized in Fig. 2 below, showing how random and new nodes are generated.

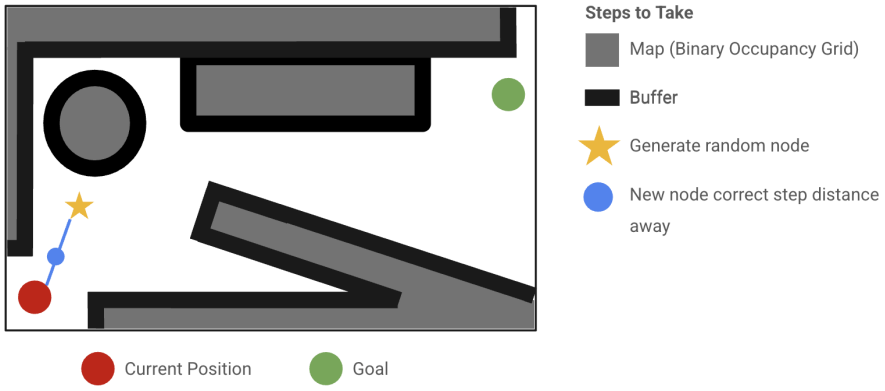

Figure 2: Random nodes are generated and new nodes are added to a tree, a given step distance away from the nearest node.

If our new node does not hit the wall, we add it to our tree. We continue to generate these random nodes until we reach the goal where we backtrack to generate our final path. Our final tree will look something like Fig. 3:

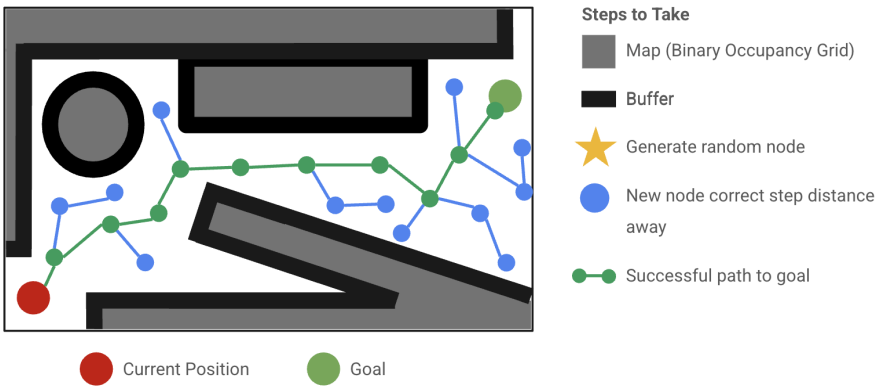

Figure 3: Our tree continues to sample the space until it reaches the goal and backtracks to create our path.

Implementing RRT helped demonstrate its advantages and disadvantages. The main disadvantage we noticed was that the generated path is not optimal, because as the number of samples increases, our solution does not necessarily converge towards an optimal path. The main advantage was time complexity; a basic RRT algorithm is $O(n \log n)$ where n depends on the number of nodes in the tree. This produced relatively fast results, with runtimes analyzed in Section 3.2. Additionally, our RRT algorithm required very little post-processing

besides backtracking to obtain our path.

2.3 Pure Pursuit Path Following

The goal of the pure pursuit path following module is to accurately follow the path generated by the path planning algorithm. The inputs to the pure pursuit are the estimated pose of the racecar from the particle filter algorithm and a list of way points from the path planning algorithm.

The path planning module outputs the path as a list of way points in x-y coordinates relative to the map frame, which the pure pursuit module listens for and stores internally. The pure pursuit module also listens for real-time pose updates from the particle filter, and when it receives one, it does the following calculations:

First, the closest line segment connecting two consecutive way points is found using matrix algebra. This function returns the index of the first way point in that segment.
Next, we compute the point of intersection of a circle of radius L_{ah}, centered at the race car's position, with the closest line segment we just found. If that line segment and circle do not intersect, we try the subsequent segments on the path until we find one that does. This intersection point is the orange "look ahead" point, as shown in Figure 3.

Given the position of the look ahead point and the position of the racecar, we calculate Δx and Δy, which is the racecar's relative position from the look ahead point.

$$\Delta x = x_{\text{lookahead}} - x_{\text{racecar}}, \tag{8}$$
$$\Delta y = y_{\text{lookahead}} - y_{\text{racecar}}. \tag{9}$$

Additionally, we know the orientation of the racecar (theta) with respect to the map frame from the pose given by the particle filter. Putting all this together, we can calculate eta, the heading of the racecar relative to the tangent line to the path at the look ahead point as follows:

$$\eta = \arctan\left(\frac{\Delta y}{\Delta x}\right) \; - \; \theta. \tag{10}$$

Now pure pursuit calculates the steering angle δ using the length of the racecar L, the relative angle η, and the lookahead distance L_{ah}.

$$\delta = \arctan\left(\frac{2\,L\,\sin(\eta)}{L_{\text{ah}}}\right). \tag{11}$$

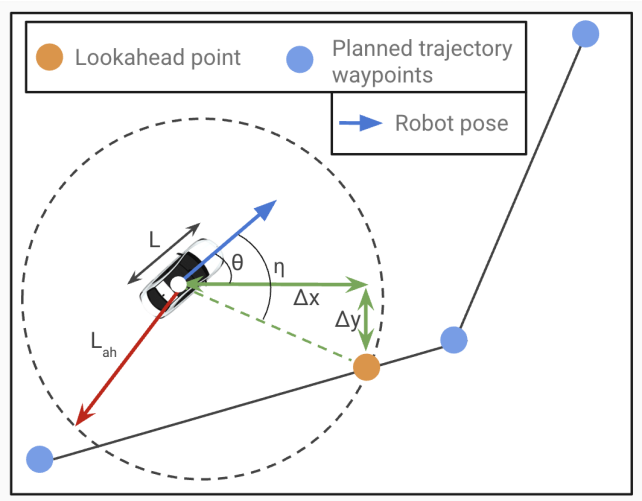

Figure 4: Pure pursuit geometry diagram. This demonstrates all the dimensions needed to solve the pure pursuit control law.

3 Experimental Evaluation

Fiona Wang, Thomas Buckley

Before we could evaluate our entire navigation stack, there were many modules and unit tests we needed to pass first. Specifically, we outlined our evaluation to be as follows:

1. **Monte Carlo Localization Evaluation in Simulation and Real World.** Our performance metrics were based on the average distance error between the estimated and ground-truth position.
2. **Path Planning Evaluation in Simulation.** We evaluated by comparing the runtime and path length of each generated trajectory
3. **Full Navigation Stack Evaluation in the Real World.** We evaluated by using cross track error.

3.1 Monte Carlo Localization Evaluation

In order to evaluate our Monte Carlo Localization, we wanted to evaluate each of our models and the particle filter in both simulation and the real world. Before testing the particle filter, we first utilized the provided unit tests to ensure that our motion and sensor models were performing without any major issues.

3.1.1 Simulation Evaluation

We evaluated our particle filter in simulation, initially using the 2D Pose Estimate tool to ensure accurate localization. After resolving early issues, we ran tests using our wall follower on two paths: Stata Path A (with turns) and Stata Path B (a straight wall). By replaying Rosbags, we visually checked if the particle cloud and odometry tracked the racecar's path, then graphed estimated vs. ground-truth positions. As shown in Fig. 5, the match was generally good.

Next, we introduced Gaussian noise to the motion model to test robustness. Higher noise led to wider particle spread, aiding recovery from divergence, while low noise caused tight convergence, risking mislocalization. We tested various noise levels and measured the mean position error, summarized in Table 1. As expected, error increased slightly with more noise, especially on Path A.

To systematically evaluate the effect of noise, we tested various values of the noise standard deviation in simulations and measured the average distance error between the particle filter's estimated position and the ground-truth position. As summarized in Table 1, the mean position error slightly increased with higher noise levels on Stata Path A, so introducing more noise naturally contributed additional uncertainty to our position estimate.

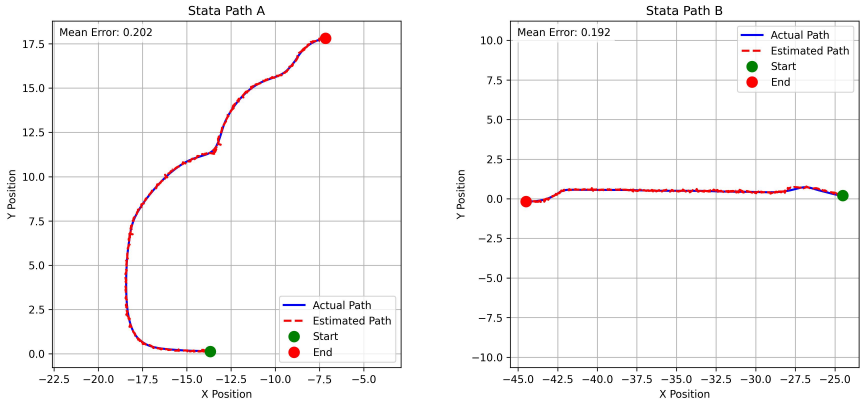

Figure 5: **In Simulation Trials.** Our localization was evaluated in simulation by running the wall follower on two paths (path a on the left and b on the right) and comparing the estimated path with the actual path (ground truth position).

Table 1: Different Values of Noise std in Motion Model on Stata Path A

x, y noise	theta noise	Error (Mean ± Std Error)
0.05	0.1	0.1273 ± 0.0539
0.10	0.1	0.1980 ± 0.0559
0.15	0.1	0.2124 ± 0.0670
0.20	0.1	0.2124 ± 0.0670

3.1.2 Real World Evaluation

In real-world tests, our particle filter quickly converged to a single pose due to a skewed initial distribution with a few high-probability particles. Resampling favored these, reducing diversity and preventing recovery from early errors.

We made three key changes to address the issue. First, we increased the motion model's noise standard deviation from 0.05 to 0.10 to improve spatial spread and robustness, keeping theta noise constant. Next, we introduced an adjustable resampling delay, which led to "pulsating" particle clusters that expanded and then converged, improving performance over resampling every update. Finally, we "squashed" the probability distribution by raising it to the $\frac{1}{3}$ power (Section 2.1.3), boosting diversity while maintaining accuracy.

To assess real world evaluation, we conducted two experiments where we recorded the path of the racecar while recording a Rosbag. We then compared the

recorded video to the estimated pose from our particle filter qualitatively. Our particle filter was highly accurate over long durations (multiple minutes) and for complex paths in the Stata basement.

3.2 Path Planning Evaluation

Next, to evaluate our path planning algorithms, we tested our RRT and A* approaches in simulation and compared their performance qualitatively as well as quantitatively through runtime and path length comparisons. Specifically, we tested using 3 different trajectories and overlayed the path generated by our RRT and A* algorithms as shown in Fig. 6. By plotting the graphs together, it is clear that A* created paths that were much smoother than RRT. Smoother paths are easier our pure pursuit to follow. In addition to the difference in smoothness, we also observed that RRT would occasionally take unnecessary turns and S-shapes, reducing its overall optimality.

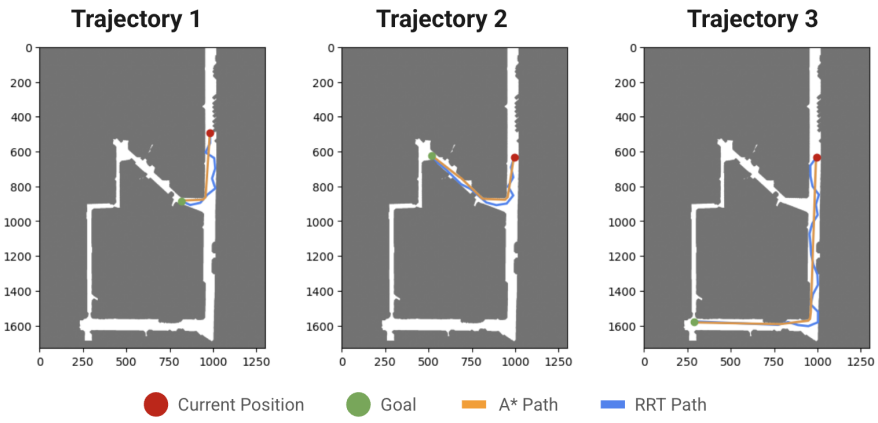

Figure 6: **Comparison of RRT and A* graphs for 3 trajectories.** Our path planning algorithms were evaluated qualitatively by running 3 unique trajectories and overlaying the results produced by RRT and A*. These graphs show how A* produced smoother, more optimized paths.

For each of the three trajectories, we also recorded the runtime and path length for RRT and A*, producing Table 2:

From all three trajectories, it is clear that RRT consistently had a shorter runtime, but A* produced shorter trajectories. From the data, we decided to implement A* on our racecar, choosing to tradeoff average runtime for smoother, shorter trajectories.

Trajectory	Runtime (sec)		Length (pixels)	
	RRT	**A***	**RRT**	**A***
1	0.094	0.431	604.341	517.157
2	0.103	0.423	840.647	771.454
3	0.153	0.454	1746.320	1607.450

Table 2: **Comparison of runtime and path length between RRT and A* for three trajectories.** These results show that RRT had shorter runtimes but A* produced shorter length paths.

3.3 Full Navigation Stack Evaluation

To evaluate the complete navigation stack, we had the racecar follow the trajectory shown in Fig. 7a. We then compared the planned trajectory to the actual trajectory (as estimated by our particle filter) every five seconds. We also computed the crosstrack error, in Fig. 7b. As shown, the racecar closely follows the path we chose. However, we found that the racecar would struggle to take hard turns. This can be seen in both figures at $t = 18$ seconds, where the racecar veers off course substantially at the turn and immediately corrects itself, causing a spike in crosstrack error.

(a) Path Planning Evaluation on Stata Path C. We compared our planned trajectory (in blue) to the estimated trajectory (in orange, particle filter) for a single path in the Stata basement (snapshot every 5 seconds).

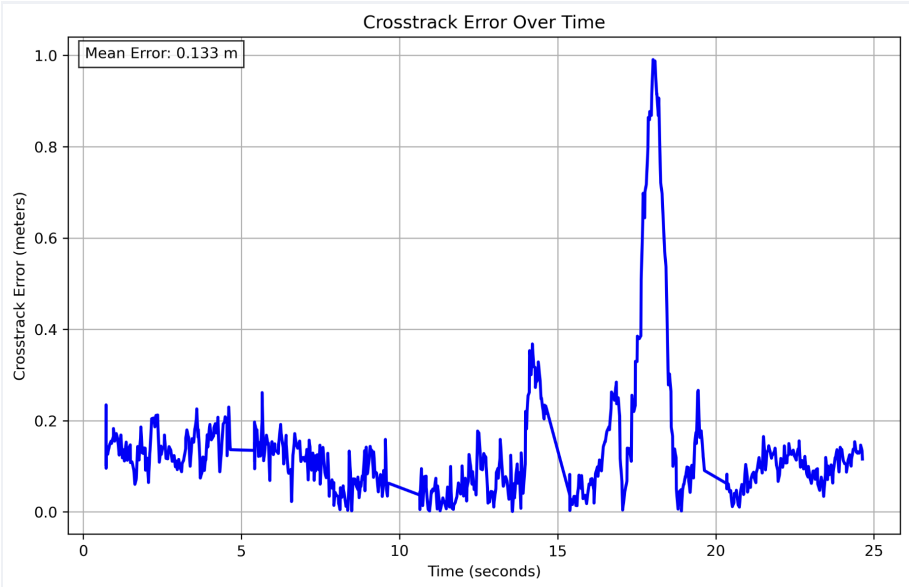

(b) Stata Path Following Crosstrack Error. We computed the crosstrack error by computing the minimum Euclidean distance to the path at each point.

Figure 7: Trajectory evaluation and crosstrack error on Stata paths.

4 Conclusion

Sriram Sethuraman

We were successfully able to integrate Monte Carlo localization, path planning,

and pure pursuit path following to enable our race car to autonomously navigate through the Stata basement. The combination of our odometry-based motion model and the LiDAR-based sensor model allowed our particle filter to effectively update an accurate estimate of the car's pose in real time. Our A* based path planning algorithm was efficiently able to plan an optimal trajectory for the racecar to follow. Using the data from the particle filter and path planner, the pure pursuit algorithm calculated the best steering angle to follow that trajectory accurately.

Qualitative analyses conducted in both simulation and the real world demonstrated our algorithm's ability to closely follow a planned trajectory. These results showed close alignment with estimated positions and planned trajectories. Quantitative results further supported our findings, showing low cross-track error between ground truth planned trajectories and estimated poses, both in simulation and real-world testing.

Future improvements will focus on tuning the system to be more effective at higher speeds, as we noticed slight oscillations after taking corners at increased speeds. This will involve tuning parameters for the localization and pure pursuit. Additionally, we plan to optimize the runtime of our path planning algorithms even further. We learned valuable technical and teamwork related lessons that we will also carry with us into the next lab.

5 Lessons Learned

Fiona Wang
This lab taught me many lessons both technical and collaborative. From a technical perspective, I learned how to implement RRT and how to optimize the paths it produced by altering the step size. I thought it was really fascinating to be able to visualize the trajectories I was creating using RViz, which not only looked cool, but was incredibly helpful for debugging my algorithm. Getting the path planning to work on simulation was super important and made transferring to the actual racecar a smooth and efficient process. Although we did not end up implementing RRT on the racecar, it was still a very rewarding project! From a collaborative standpoint, I thought that our team organization was super effective this week. We were able to split up the map callback, two path planning algorithms, and pure pursuit between the four of us and convened to implement everything onto the racecar. Our timelines matched up super well and everyone used their time effectively. This was the first lab that we finished early, giving us more time to perfect our briefing slides.

Ben Lammers
I learned real-world applications of my prior autonomy coursework. While initially A* seemed like a brute-force, crude solution, implementing the algorithm and seeing it deliver optimal results made it feel more viable to me. From a

communication perspective, I learned the importance of sticking to deadlines in a group. Multiple times, my teammates and I ran up until the very end of deadlines because of our procrastination. In the future, I plan to set early deadlines for different deliverables, such that our team has a buffer between when things are completed and when things are due.

Thomas Buckley
During this lab, I gained insight into the value of having a standardized testing methodology and clearly defined evaluation pipelines. As our system continues to grow in complexity, consistently and accurately assessing performance becomes increasingly challenging. For example, we needed to run many systems at the same time (localization, simulator, wall_follower, the evaluation pipeline), as well as have a standardized starting and ending position for the car. Additionally, as system complexity grows, we needed to be more creative in our evaluation metrics (especially in the real-world where we can't easily obtain a ground truth for racecar position). Building out a scalable way to do this evaluation was difficult, but helped us rapidly evaluate racecar parameters which will save time later on.

Sriram Sethuraman
A robust understanding of the math behind the algorithms we are implementing makes the programming and debugging much more efficient. I also learned that communication of progress and code comments are very important so we know what work has been done and we don't do any redundant work. And lastly, when we worked in parallel we were able to get a lot of things done very efficiently.